Improved Cryogenic Current Comparator Setup With Digital Current Sources

Martin Götz, Dietmar Drung, Eckart Pesel, Henry-Jobes Barthelmess, Colmar Hinnrichs, Cornelia Aßmann, Margret Peters, Hansjörg Scherer, Bernd Schumacher, and Thomas Schurig

***Abstract*—We have realized an improved resistance calibration setup based on a cryogenic current comparator (CCC). The new comparator with 18 windings and a total of 4647 turns suits well for all the necessary comparisons of a 100-Ω standard resistor with the quantum Hall effect (QHE) and within the range of standard resistance values from 1 Ω to 1 MΩ. The new state-of-the-art setup is equipped with a dc Superconducting Quantum Interference Device (SQUID) and a digital double current source, allowing a reduction in the ramping time by at least one order of magnitude and significantly improving the dynamic stability of the system. The latter also benefits from the internal wideband feedback that we present in this paper.**

***Index Terms*—Current comparators, feedback circuits, magnetic shielding, resistance measurements, Superconducting Quantum Interference Device (SQUID).**

I. Introduction

ULTIMATE precision in resistance comparison—a few parts in 10^9 at best—is achieved with measurement setups based on cryogenic current comparators (CCCs) [1]. For this reason, CCCs are preferably used for resistance calibration at national metrology institutes, including the Physikalisch-Technische Bundesanstalt (PTB) [2]. According to international agreement, the unit of electrical resistance, i.e., the ohm, is bindingly fixed to the quantum Hall effect (QHE), providing the conventional value $R_{K-90} = 25.812807\,\mathrm{k\Omega}$ [3]. In practice, a 100-Ω standard resistor achieves its traceability from a comparison with a QHE resistance of 1/2 R_{K-90} at a filling factor of $i = 2$. Subsequently, starting from this 100-Ω resistor, one can scale to lower and higher values as we do in the calibration of standard resistors ranging from 1 Ω to 1 MΩ and resistors of 25 Ω used in thermometry. Resistance calibration thus requires, at the least, the determination of resistance ratios of 4, 10, 100, and 129.064035 to 1 with the highest accuracy.

Reconsidering our measurement capabilities, we intended to replace the two first-generation CCC setups used so far by one state-of-the-art system, including a dc Superconducting Quantum Interference Device (SQUID), instead of a RF SQUID, and a digital double current source (DCS), instead of the precursory analog DCS. Therewith, the work described here joins a trend that started at other metrology laboratories several years ago (cf., e.g., [4] and [5]). The focus of our development was placed on the significant reduction in the overall measurement time. In particular, current reversal should be performed much faster, thus putting requirements on the operation of the SQUID, which should remain locked during the fast reversal.

The measurement conception is summarized in Section II. In Section III, a detailed discussion of the stability of the SQUID-based feedback and how it benefits from a technique we call internal wideband feedback (IWF) is presented. In Section IV, we present the technical details of the new setup and preliminary measurement results. We give the conclusion in Section V.

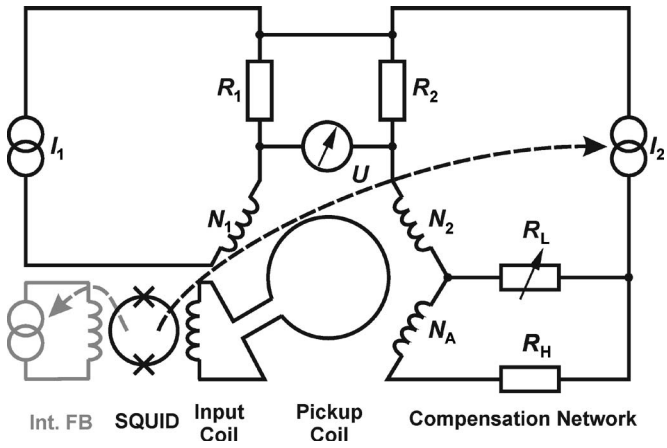

Fig. 1. Simplified scheme of the setup. The DCS-generated currents I_1 and I_2 cause voltage drops across the resistors to be compared, i.e., R_1 and R_2. The difference U of both these voltage drops is measured by a nanovoltmeter. Also flowing through CCC windings with numbers of turns N_1 ("primary circuit") or N_2 and N_A ("secondary circuit"), respectively, I_1 and I_2 generate an overall magnetic flux that is coupled into the SQUID loop via pickup coil and input coil. Feeding back the SQUID signal to one of the current sources (dashed black arrow), the total flux generated in the CCC and, hence, the ratio of I_1 and I_2 are kept constant at a value determined by the numbers of turns and by the resistances R_L and R_H of the compensation network included in the secondary circuit. In the lower left corner, the circuit displayed in gray represents an additional feedback path via the integrated feedback coil, which is used to realize an IWF.

II. Concept of the Measurement Setup

A. Resistance Bridge

The scheme of our CCC-based resistance bridge is shown in Fig. 1. The resistance ratio R_1/R_2 to be determined is

Manuscript received June 10, 2008; revised December 19, 2008. First published February 13, 2009; current version published March 10, 2009. The Associate Editor coordinating the review process for this paper was Dr. Yi-hua Tang.

M. Götz, E. Pesel, H. Scherer, and B. Schumacher are with the Physikalisch-Technische Bundesanstalt, 38116 Braunschweig, Germany (e-mail: martin.goetz@ptb.de).

D. Drung, C. Aßmann, M. Peters, and T. Schurig are with the Physikalisch-Technische Bundesanstalt, 10587 Berlin, Germany.

H.-J. Barthelmess and C. Hinnrichs are with Magnicon GbR, 22397 Hamburg, Germany.

Digital Object Identifier 10.1109/TIM.2008.2012379

0018-9456/$25.00 © 2009 IEEE

calculated from the (reverse) ratio of dc bias currents I_1 and I_2 and from the imbalance of the bridge represented by the ratio of voltage U and voltage drop I_2R_2 across one of the resistors as

$$\frac{R_1}{R_2} = \frac{I_2}{I_1} \cdot \left(1 - \frac{U}{I_2 R_2}\right). \quad (1)$$

Unparalleled by any other current comparator, a CCC enables the realization of a dc current ratio with better accuracy than one part in 10^9. For the sake of a minimum overall uncertainty, the contribution U/I_2R_2 in (1) must be kept as small as possible, requiring the reverse current ratio to adequately approach the real resistance ratio. In our setup, this is achieved by including a compensation network into the secondary circuit.

B. CCC and Compensation Network

As the basic feature of a CCC, for a given current I, the magnetic field outside the toroidal superconducting screen is strictly proportional to the number of turns N through which this current is flowing, i.e., the dependence of the outer magnetic field on the inner topology of the windings is negligibly small. For a properly designed CCC, this holds down to a level of one part in 10^{10}. Outside of the overlapped shield, the net magnetic flux from two currents of opposite direction will cancel if and only if their magnitudes are of the reverse ratio of the respective numbers of turns. Feeding back the signal of a suitably placed SQUID magnetometer (acting as the null detector), one can keep the ratio of the currents fixed to the reverse ratio of the integer numbers of turns.

With a maximum overall number of turns of a few thousands, balancing of the resistance bridge by choosing appropriate numbers of turns N_1 and N_2 is limited to several parts in 10^4, which is not sufficient with respect to the uncertainty contribution of the bridge voltage previously considered. For finer tuning of the effective ratio of the numbers of turns, we apply an auxiliary winding with N_A turns and a compensation network [3] shown in Fig. 1. The resistance ratio is calculated as

$$\frac{R_1}{R_2} = \frac{N_1}{N_2} \cdot \left(1 - \frac{U}{I_2 R_2}\right) \cdot \left(1 \pm \frac{N_A}{N_2} \cdot \frac{R_L}{R_H + R_L}\right)^{-1} \quad (2)$$

with the sign of the N_A term depending on the parallel or the antiparallel orientation of the magnetic fields generated in the two secondary coils. In our measurements, N_A/N_2 is equal to 2; typically, R_H is 10 MΩ and R_L is a three-digit resistance decade with an increment of 0.2 Ω, enabling a balance of the resistance bridge of about four parts in 10^8 or better, i.e., for a typical voltage drop I_2R_2 of 0.5 V, the bridge voltage can be reduced to a few tens of nanovolts.

C. Reversal of Current Direction

Even under advanced laboratory conditions, including ambient temperature stabilization of better than ± 0.5 K, the measurement of a bridge voltage at the nanovolt scale is affected by drifts of thermal voltages. To get rid of this parasitic effect, the directions of the primary and secondary currents are simultaneously reversed at a timescale that justifies the treatment of the thermal voltages as a linear drift. In (2), one then finally has to replace U and I_2R_2 by ΔU and $\Delta(I_2R_2)$, i.e., the average differences between the bridge voltage or the voltage drop across the secondary resistor, respectively, as obtained by a series of measurements with alternating current directions. The demands on the feedback dynamics will be included in the discussion in the next section.

III. SQUID-BASED FEEDBACK

The dc SQUID is an ultrasensitive magnetic flux-to-voltage converter: The voltage V across a superconducting loop interrupted by two weak links (Josephson junctions) periodically depends on the magnetic flux Φ penetrating the SQUID loop with a period given by the magnetic flux quantum Φ_0 of about $2 \cdot 10^{-15}$ Wb.

Starting from the SQUID providing voltage change ΔV caused by a change $\Delta\Phi$ in the magnetic flux, a feedback loop can be realized by adding an amplifier, followed by an integrator, and driving a current proportional to the integrator's output voltage through a coil that is inductively coupled to the SQUID loop. For feedback purposes, a thin-film coil is usually integrated on the SQUID chip ("integrated feedback coil"), but any other coil with sufficiently strong coupling to the SQUID loop will also be suitable. In the scheme considered here (see Fig. 1), the CCC windings of the secondary circuit are used as the feedback path for keeping the stationary magnetic flux component generated in the whole CCC constant ("external feedback"). After closing this feedback loop when I_1 and I_2 are both zero, the net flux through the detector loop will be held constant, and the application of opposing currents I_1 and I_2 and the reversal of these currents should not affect the balance condition. However, away from this ideal situation, in a real experiment, one usually faces four problems.

1) Magnetic fields in the environment, i.e., from any source other than the currents in the CCC, will directly be picked up by the SQUID and, hence, indistinguishably interfere with the CCC-generated signal.
2) Noise currents in the windings, as generated by the dissipative elements of the electrical circuit connected to the CCC (e.g., by the resistors to be compared) or pick-up noise contributions, will finally produce additional flux noise in the SQUID.
3) If made of a low-resistance or superconducting material, the CCC with the distributed capacitances and inductances along the wires is an oscillating system that, at finite temperature or after other excitation, provides parasitic dynamic input to the feedback loop (which is the so-called *LC* self-resonance at, typically, a few tens of kilohertz).
4) In the course of reversing the current directions, transient distortions might become critical with respect to the stability of the SQUID's lock point, i.e., the point at its $V-\Phi$ characteristic where the SQUID is operated.

In summary, interfering external signals and both the dynamic and noise limitations of proper SQUID feedback have

to be carefully analyzed. Magnetic shielding is conventionally achieved by a combination of a high permeability and a superconducting screening cup, as will be briefly sketched later in this paper. The effects related to noise and transients will be discussed in more detail here.

A. Noise, LC Self-Resonance, and Transients

Even assuming the SQUID magnetometer (consisting of the SQUID loop and the input and pickup coils) to be located at a magnetically perfectly shielded place, the voltage across the SQUID will display noise. Essentially, the intrinsic noise of the SQUID sensor (including its readout electronics), the external noise coupled into the pickup coil via the CCC ("indirect pickup"), and the noise generated in the CCC will contribute to the total noise. With respect to the signal-to-noise ratio, only the first contribution depends on the overall coupling between the CCC and SQUID loop: The sensor-related noise will become limiting only for very weak coupling; otherwise, as in our case, the CCC-related noise sources will dominate. For the setup under consideration, we found a significantly increased noise level for the SQUID magnetometer in the CCC probe, as compared with the values obtained from a precharacterization of the bare SQUID. As shown in Fig. 2(a), the flux noise increases from 3.4 $\mu\Phi_0/\mathrm{Hz}^{1/2}$ to about 10 $\mu\Phi_0/\mathrm{Hz}^{1/2}$ at 1 Hz and from 8.1 $\mu\Phi_0/\mathrm{Hz}^{1/2}$ to about 20 $\mu\Phi_0/\mathrm{Hz}^{1/2}$ at 0.1 Hz. This noise should be compared to the total flux signal in the CCC. In a typical measurement, ± 80 mA $\cdot$ turns are applied in the primary and secondary windings. A transfer coefficient of 10.44 μA $\cdot$ turns$/\Phi_0$ corresponds to a flux change of $1.53 \cdot 10^4\ \Phi_0$ when reversing I_1 and I_2.

The spectral distribution of the overall noise in the magnetometer-plus-CCC configuration is shown in Fig. 2(a). An excess low-frequency noise of below 1 Hz is found as usual in the dc SQUID spectra. The increased noise level up to several hundreds of hertz is not fully understood yet; presumably, mechanical vibrations are involved here. As a peculiarity, one finds a narrow-band noise peak at 41 kHz in the spectrum of Fig. 2(a). This additional noise contribution (not found for the bare SQUID) results from the thermal excitation of the *LC* self-resonance in the CCC windings. In particular, during the ramp, transients can strongly excite this high-quality resonator, thereby degrading the stability of the feedback loop. In some cases with high ampere-turns levels, we observed such a reduction in the stability. This situation can be improved by damping the *LC* self-resonance. As an alternative to the use of resistive wire (cf. [6]), we connect an *RC* series circuit to an additional CCC winding. The effect of this damping is shown in Fig. 2(b): Compared with the undamped configuration in Fig. 2(a), the quality factor of the resonance peak is significantly reduced. However, aside from this intended improvement, the integral noise increases, because the resistor, which is the necessary dissipative element, also acts as an additional noise source. The resulting high-frequency excess noise can strongly be reduced by placing the *RC* circuit in the low-temperature part of the probe, as clearly shown in Fig. 2(b). Note that, due to the decoupling of the series capacitor, the noise level at low frequencies (including the frequency of current reversal as the fundamental frequency here) is not affected by this extra noise generation. Moreover, the technique that we describe in the next section enables an efficient dynamic suppression of noise components of up to several hundreds of kilohertz.

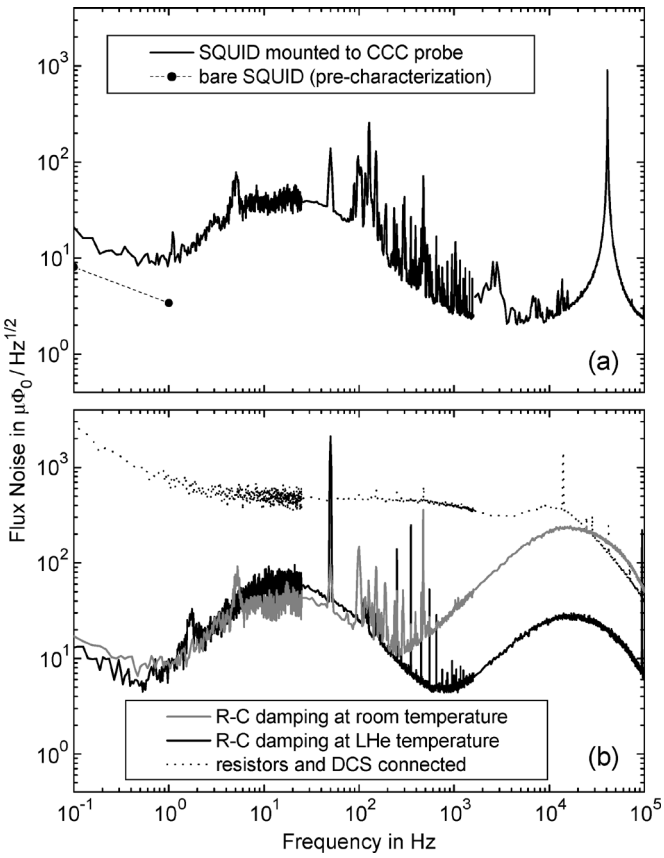

Fig. 2. SQUID noise spectra. The original noise spectrum of the SQUID magnetometer mounted on the CCC probe shown in (a) displays a prominent peak at 41 kHz. In (b), we present the spectra when damping this high-quality *LC* self-resonance by connecting an *RC* circuit (240 Ω in series with 100 nF) to a 256-turn winding. In recording both of these spectra, resistors and current sources have been disconnected from the CCC. The spectrum when connecting resistors of 100 Ω and 10 kΩ and the current sources (operated at 5 mA and 50 μA, respectively) is shown in (b) for the case of "warm" *RC* damping. Note that the extra noise of the current sources does not affect the bridge voltage, because it is canceled out by the SQUID via the external feedback loop.

B. Internal Wideband Feedback

Our SQUID readout electronics XXF-1 [7] does not involve flux modulation. Instead, additional positive feedback (APF) [8] is used to suppress the noise of the room-temperature amplifier. As shown in Fig. 1, there are two more feedback paths available, namely, via the integrated feedback coil ("internally") or via the secondary CCC windings and the pickup and input coils ("externally").

With the ultrafast SQUID electronics we use, an internal feedback bandwidth of up to 20 MHz can be chosen. Differing from that, in the external feedback loop, phase stability requires a bandwidth limitation to a few kilohertz in view of the CCC's self-resonance (regardless of being damped or not) and even lower cutoff frequencies of other elements in the loop, e.g., the indispensable isolation amplifier. On the other hand, Fig. 2(b)

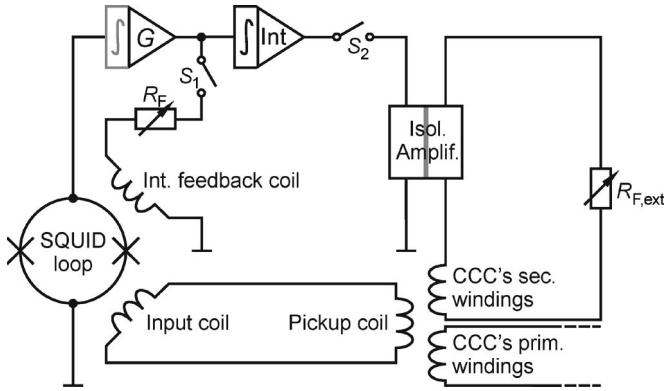

Fig. 3. Feedback scheme. The magnetic flux through the SQUID loop is kept constant via the integrated feedback coil (with amplifier G as an integrator with quasi-infinite dc gain and with switches S_1 and S_2 closed and open, respectively) or the external feedback path (with an amplifier G with fixed gain, S_1 open but S_2 closed). For resistance comparison, external feedback is used (with S_2 closed), but the IWF is activated by also closing S_1 and operating G as an amplifier with finite bandwidth. For the sake of simplicity, the APF is not shown in this scheme.

shows the presence of a considerable noise contribution above this bandwidth, which cannot be canceled in this feedback regime. As a result, there is a considerable amount of uncompensated flux noise "seen" by the SQUID, which can readily exceed the linear flux range and increase the SQUID noise by mixing-down effects.

As an appropriate solution, we introduce the IWF scheme, as shown in Fig. 3. The basic idea is to simultaneously use two feedback paths but for different purposes, i.e., via the internal path, a negative feedback with finite gain and bandwidth (typically 200 kHz) overcompensates the APF and provides a wideband suppression (by a factor of about 6) of dynamic input signals covering the critical frequency range previously discussed. With the frequency-independent gain of below 200 kHz, the IWF acts in the same way (but with different sign) as the APF, i.e., the combination of both simply results in a modified $V-\Phi$ transfer coefficient in the working point (specific to the IWF settings). The external feedback, including the only integrator, then controls the very-low-frequency signals, i.e., those arising from the quasi-stationary currents I_1 and I_2 in the primary and secondary circuits, which represent the essential mechanism for keeping the current's ratio constant.

Altogether, the IWF reduces the level of wideband noise "seen" by the SQUID, thus providing a valuable increase in the dynamic stability of the external feedback. For typical IWF settings, we find an overall linear flux range of about $\pm 0.2\Phi_0$. Note that the IWF does not increase the flux noise contribution of the room-temperature amplifier (see G in Fig. 3).

IV. Details of the New Setup

A. Design of CCC, SQUID, and Probe

With our type-I CCC [9], one can select from a set of 18 different windings at room temperature. The numbers of turns range from $2^0 = 1$ to $2^{11} = 2048$. Additional windings of 1, 2, 4, 16, 17, and 512 turns are available. These windings can freely be combined to build the needed set of numbers N_1, N_2, and N_A and realize *RC* damping of the self-resonance at room temperature. Alternatively, an additional 256-turn winding is destined for *RC* damping at 4.2 K.

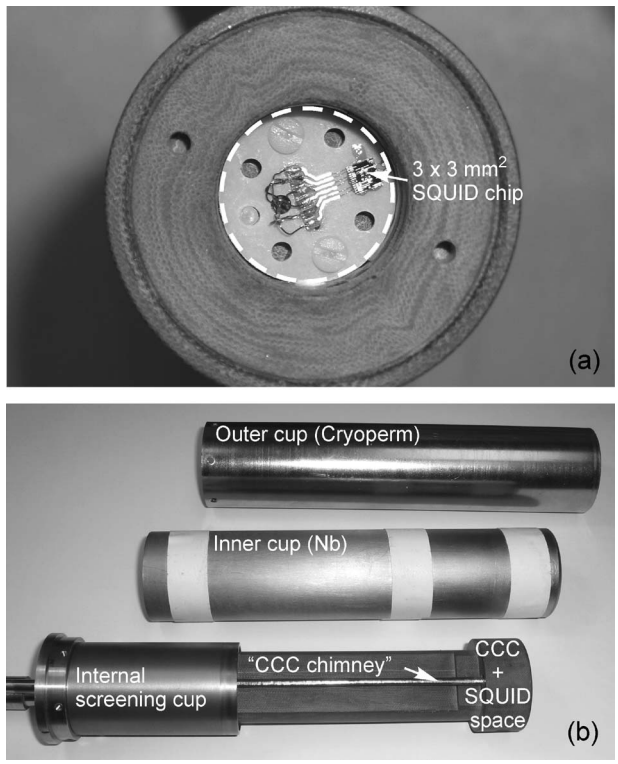

Fig. 4. Low-temperature end of the probe. (a) Support for the CCC and the SQUID chip seen from the bottom end; this support is made of laminated fabric. The dashed line denotes the pickup coil's position and approximate size. (b) Two overall screening cups and the inner parts. The Cryoperm and niobium cups have inner diameters of 45 and 42 mm, respectively; the inside height of the niobium cup is 188 mm. The internal screening cup is also made of niobium. It consists of a base plate and a hollow cylinder joined by a thread.

We use NbTi in a copper matrix as the wire material for the CCC windings. The overall diameter of this wire is 70 μm (including insulation). The superconducting screen of the CCC is overlapped 2.7 times and is made of lead; the outer diameter of the torus is 31.4 mm.

The PTB-made SQUID chip (with integrated feedback and input coils) is glued onto a plastic carrier that exactly fits into the opening of the CCC torus [18.4 mm in diameter; see Fig. 4(a)]. On the rear side of the chip carrier, an 18-mm-diameter groove takes a 0.25-mm niobium wire, which is the single-turn pickup coil. This way, we obtain a SQUID magnetometer with a sensitivity of about 0.6 nT/Φ_0. The SQUID carrier is inserted into the CCC's opening up to the middle plane.

For effective shielding from external magnetic fields, the most sensitive components are placed close to the bottom of a pair of screening cups [see Fig. 4(b)]. The 1-mm-thick outer cup is made of Cryoperm, which is an alloy with high permeability even at liquid-helium temperature, whereas the niobium-made inner cup is a superconducting screen. In addition, the internal niobium screening cup [see Fig. 4(b)] shields the lower part of the cup from the upper part, which contains printed circuit boards for connecting the wire ends of the CCC windings with the leads from room temperature.

B. Double Current Source

The design of the new digital DCS started from an analysis of the existing pair of throughout analog DCSs. Obviously, damping and the IWF can considerably improve the situation, but most of the sources of dynamic instability have been related to the old DCS design. This concerned, mainly, stray-charge effects when driving switches during current reversal and, speaking more generally, any temporary flux imbalance while simultaneously ramping the primary and secondary currents. As a rather conservative rule of thumb, one has to keep the dynamic deviation during current reversal safely below 1/4 Φ_0 to remain locked. To reduce the measurement time in the new setup, we minimize the dynamic deviations to allow for a high ramping speed.

The core element of each current source is a microcontroller-operated 16-bit digital-to-analog converter (DAC). After passing through a 1-kHz low-pass filter, the output signal feeds an analog voltage-driven current source based on operational amplifiers. The current source modules are separately housed in closed metallic boxes, which are insulated (Teflon) from each other, from the control unit (CU) module, and from the common 19-in mainframe shared by all these modules. In combination with the RF filters at the outputs of the current sources, the hermetic enclosure of the modules minimizes the detrimental effect of RF interference.

The CU also contains a microcontroller, which communicates with the computer via a universal serial bus interface and the current source modules via optical fibers. From the CU, the microcontrollers of the current source modules receive all the information about the ramp settings (i.e., ramping amplitude and time, digital increment, optional delay, and offset) and a triggering signal preceding any ramping. Each of the three modules has its own lead storage battery. Charging is managed by the CU; it is not carried out during measurements.

Temporary flux imbalance during ramping is reduced to a tolerable level by synchronous operation of the current sources. For this purpose, the DACs of both sources are simultaneously incremented or decremented, respectively, with the same step size (selectable from 1, 2, 4, 8, ..., 8192 LSB). Hence, for a given ramp, the total number of DAC increments or decrements is identical for both current sources, and the ratio of the output currents is the same as the ratio of the full-scale currents of the sources. At present, the following six main current ranges are available in both source modules: ± 10 μA, ± 77.481 μA, ± 100 μA, ± 1 mA, ± 10 mA, and ± 100 mA. Based on these main ranges, additional subranges (dividing the full-scale output of a main range by an integer number 2, 3, ...) can be selected. An offset correction of up to about $\pm 2\%$ of the source range can also be chosen.

Each current source is equipped with a quartz clock; the periods of these quartz clocks are tuned to agree sufficiently well to avoid the critical divergence of the times of DAC operation during ramping. The time required for changing a DAC output value is about 41 μs, i.e., even for the minimum step size of 1 LSB, a full-scale ramp can be performed in about 2.6 s. Ramping of both current sources is triggered by the CU's microcontroller, but an adjustable delay between the two ramps can be set for adaptation to different reactances in the primary and secondary circuits. This way, we can reduce dynamic deviations during the ramps. When ramping, the communication with the source modules is suspended; after reaching the target level of the DAC ramp, a signal is sent back to the CU.

One of the current source modules is prepared for the injection of the feedback signal generated by the SQUID electronics. To achieve the necessary electrical isolation, this signal is converted into a sequence of voltage pulses via a voltage-to-frequency converter. After optical transmission, it is passed through a frequency-to-voltage converter, followed by a digitally controlled voltage divider. The latter device offers an attenuation that can be chosen in 16 steps between 1 : 1 and 1 : 32 768. The output voltages of this voltage divider and the 16-bit DAC are superimposed, the resulting voltage finally controls the output current of this source module. Note that the attenuation affects both the range and the bandwidth of the external feedback loop.

C. Preliminary Results

For a first test, we compared a well-known 100-Ω standard resistor with the 12.9064035 kΩ provided by the QHE at $i = 2$. Specific to this configuration, the cable between the CCC and QHE setups is considerably long (about 20 m).

Prior to the measurements, we have analyzed the margins of stable feedback operation, i.e., we determined the ramp's maximum step size for a given feedback strength. For a number of attenuator ratios, we could drive the ramps with a step size of up to 16 LSB. This corresponds to an overall ramping time of about 163 ms, during which the magnetic flux signals coupled into the SQUID loop from both circuits are changed by about 15 300 flux quanta in a sufficiently well-synchronized way to keep the SQUID's working point stable. The wait time between the data acquisitions for consecutive cycles with different current directions could be chosen to be as small as 2.5 s, corresponding to ten time constants of the nanovoltmeter operated at maximum bandwidth.

In Fig. 5, we present the measurement data obtained with the new CCC probe, in combination with the new DCS. The resistance ratio calculated from these data agrees within one part in 10^8 with the results of measurements performed with the previously established setup. The reason for this difference is currently under investigation.

V. Conclusion

The new setup's figure of merit is a significantly increased ramping speed. The basis of this improvement is the synchronized DAC-controlled ramping of the primary and secondary currents and proper matching of the SQUID-based feedback. The dynamic stability of SQUID operation notably benefits from the *RC* damping of the CCC's self-resonance, combined with the IWF. Moreover, the compact design of the setup makes it less sensitive to pickup of distorting signals (e.g., at power line frequency). At the next stage of extension, the nanovoltmeter used so far (EM N11) will be replaced by an

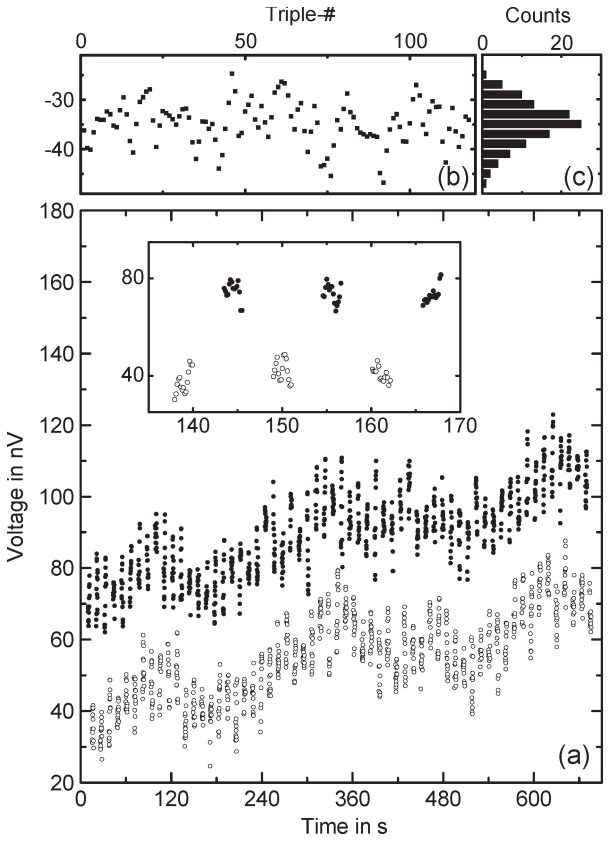

Fig. 5. Comparison of a 100-Ω standard resistor with the QHE $(i = 2)$ using the new CCC probe $(N_1 = 2065,\ N_2 = 16,$ and $N_A = 32)$ and the new current source $(\Delta(I_2R_2) = 987.6$ mV). The step size of the ramps was 8 LSB (i.e., the ramping time is about 0.33 s); the 1:8 attenuation of the feedback signal corresponds to about 340-Hz bandwidth in the external feedback loop. The frequency of current reversal was 94 mHz. (a) Bridge voltage recorded for a sequence of 120 cycles with alternating current directions (filled or hollow dots, respectively). (b) Single values of the bridge voltage difference ΔU_i obtained for the 118 triples of consecutively acquired cycles. (c) Histogram of all the ΔU_i values; the mean bridge voltage difference ΔU is calculated to be -34.8 nV with a standard deviation of 0.7 nV. The resistance ratio was calculated to be 129.06394656 with a type-A uncertainty $(k = 2)$ of 1.5 parts in 10^9.

instrument that is also included in the mainframe. This could allow for further reduction in the wait time down to tenths of a second and would minimize the time intervals, which do not contribute to the integration time of the nanovoltmeter. Moreover, for enabling fully automated measurements, we plan to realize a microcontroller-operated compensation module that is based on an R–2R network and placed in the mainframe. Compared with our previous setups, the flexibility with respect to the resistance ratios to be determined is highly increased. This possibly offers interesting applications, e.g., in thermometry. The digital DCS described in this paper and the SQUID electronics are commercially available [10].

ACKNOWLEDGMENT

The authors would like to thank J. Beyer, R. E. Elmquist, R. Grill, L. Palafox, H. K. Singh, and P. Warnecke for fruitful discussions and M. Britze, V. Bürkel, M. Busse, and G. Muchow for excellent technical support.

REFERENCES

[1] I. K. Harvey, "A precise low temperature dc ratio transformer," *Rev. Sci. Instrum.*, vol. 43, no. 11, pp. 1626–1629, Nov. 1972.
[2] F. Delahaye, T. J. Witt, E. Pesel, B. Schumacher, and P. Warnecke, "Comparison of quantum Hall effect resistance standards of the PTB and the BIPM," *Metrologia*, vol. 34, no. 3, pp. 211–214, 1997.
[3] B. Jeckelmann and B. Jeanneret, "The quantum Hall effect as an electrical resistance standard," *Rep. Prog. Phys.*, vol. 64, no. 12, pp. 1603–1655, Dec. 2001.
[4] P. Kleinschmidt, J. M. Williams, N. E. Fletcher, and T. J. B. M. Janssen, "Cryogenic current comparator bridge for quantum Hall resistance ratio measurements," *Proc. Inst. Elect. Eng.—Sci. Meas. Technol.*, vol. 149, no. 6, pp. 302–304, Nov. 2002.
[5] G. Rietveld, J. M. Williams, E. Houtzager, and T. J. B. M. Janssen, "Automated CCC bridge for precision resistance measurements," in *CPEM Conf. Dig.*, 2006, pp. 496–497.
[6] R. E. Elmquist, E. Hourdakis, D. G. Jarrett, and N. M. Zimmerman, "Direct resistance comparisons from the QHR to 100 MΩ using a cryogenic current comparator," *IEEE Trans. Instrum. Meas.*, vol. 54, no. 2, pp. 525–528, Apr. 2005.
[7] D. Drung, C. Hinnrichs, and H. J. Barthelmess, "Low-noise ultra-high-speed dc SQUID readout electronics," *Supercond. Sci. Technol.*, vol. 19, no. 5, pp. S235–S241, May 2006.
[8] J. Clarke and A. I. Braginski, Eds., *The SQUID Handbook*. Weinheim, Germany: Wiley-VCH, 2004, pp. 141–143.
[9] D. B. Sullivan and R. F. Dziuba, "Low-temperature direct-current comparators," *Rev. Sci. Instrum.*, vol. 45, no. 4, pp. 517–519, Apr. 1974.
[10] [Online]. Available: www.magnicon.com

Martin Götz was born in Erfurt, Germany, in 1968. He received the Diploma and Ph.D. degrees in physics from the University of Jena, Jena, Germany, in 1992 and 1997, respectively.

After his research at the University of Karlsruhe, Karlsruhe, Germany, and the University of Chemnitz, Chemnitz, Germany, he joined the Physikalisch-Technische Bundesanstalt, Braunschweig, Germany, in 1999. His previous research interests included thin-film technology, single-charge phenomena, and the Josephson effect. He is currently working on electrical quantum metrology.

Dietmar Drung received the Dipl.-Ing. and Dr.-Ing. degrees in electrical engineering from the University of Karlsruhe, Karlsruhe, Germany, in 1982 and 1988, respectively.

From 1983 to 1988, he was a Researcher with the University of Karlsruhe, where he worked on digital and analog circuits with Josephson junctions. In 1988, he joined the Physikalisch-Technische Bundesanstalt, Berlin, Germany, where he is working on superconducting quantum interference devices (SQUIDs) and measurement systems for magnetic sensing and electrical metrology. He contributed a number of new concepts to improve the performance and user-friendliness of SQUID sensors. His research interests include the development of high-performance dc SQUID readout electronics and low-noise amplifiers.

Eckart Pesel was born in Uelzen, Germany, on April 15, 1960. He received the Dipl.-Ing. (FH). degree from the Fachhochschule Wolfenbüttel, Wolfenbüttel, Germany, in 1990.

In 1990, he joined the Physikalisch-Technische Bundesanstalt, Braunschweig, Germany, where he is working on the quantum Hall effect and the development of the cryogenic current comparator.

Henry-Jobes Barthelmess was born in Düsseldorf, Germany, in 1969. He received the Diploma degree in physics from the Technical University of Berlin, Berlin, Germany, and the University of Hamburg, Hamburg, Germany. He defended his Ph.D. dissertation about high-Tc superconducting quantum interference devices at the Institute of Applied Physics, University of Hamburg, in 2002.

In 2000, he cofounded Magnicon GbR, Hamburg, where he is currently a Codirector.

Colmar Hinnrichs was born in Hamburg, Germany, in 1966. He received the Diploma degree in physics from the University of Hamburg, Hamburg, where he has been working on magnetic field sensors.

In 2000, he cofounded Magnicon GbR, Hamburg, where he is currently a Codirector.

Cornelia Aßmann received the Dipl.-Ing. degree in electronic technology from Humboldt University of Berlin, Berlin, Germany, in 1986.

From 1986 to 1991, she was with the Federal Institute for Standardization, Metrology, and Product Testing (ASMW). In 1991, she joined the Physikalisch-Technische Bundesanstalt, Berlin, working on the fabrication and application of superconducting sensors.

Margret Peters received the Dipl.-Ing. (FH) degree in physical technology from Fachhochschule Lübeck, Lübeck, Germany, in 1983.

In 1983, she joined the Physikalisch-Technische Bundesanstalt, Berlin, Germany, where she worked on the microfabrication of superconducting quantum interference device sensors for magnetic sensing and electrical metrology. Her research interests include the development and supply of microfabrication technology (i.e., lithography, sputtering, etch techniques, and cleanroom engineering).

Hansjörg Scherer was born in Germany in 1965. He received the Diploma and Ph.D. degrees in physics from the Technical University of Braunschweig, Braunschweig, Germany, in 1992 and 1995, respectively.

In 1992, he joined the Physikalisch-Technische Bundesanstalt (PTB), Braunschweig, where he has been working on single-electron tunneling since 1995. He is currently the head of a working group in the field of single-electron tunneling, electrical current, and charge. His research interests include quantum electronics and quantum metrology.

Bernd Schumacher was born in Aachen, Germany, on July 9, 1960. He received the Dipl.-Ing. and Dr.-Ing. degrees from the University of Technology, Aachen, in 1986 and 1991, respectively.

In 1991, he joined the Physikalisch-Technische Bundesanstalt, Braunschweig, Germany, where he is working on the quantum Hall effect, cryogenic current comparators, and the calibration of resistance standards.

Thomas Schurig received the Diploma degree in physics, the Dr. rer. nat. degree in experimental physics, and the Dr. sc. nat. degree in natural sciences from Humboldt University of Berlin, Berlin, Germany, in 1979, 1982, and 1989, respectively.

During 1981–1991, he was with Humboldt University of Berlin, studying low-temperature solid-state physics. In 1991, he joined the Physikalisch-Technische Bundesanstalt, Berlin, where he worked on superconducting sensors. He is currently heading the Department of Cryo- and Vacuum Physics.